

## Experimental and theoretical studies of acetylene layers adsorbed on KCl(001)

A. L. Glebov, V. Panella, J. P. Toennies, F. Traeger, and H. Weiss  
*Max-Planck-Institut für Strömungsforschung, Bunsenstr. 10, D-37073 Göttingen, Germany*

S. Picaud, P. N. M. Hoang, and C. Girardet  
*Laboratoire de Physique Moléculaire, UMR CNRS 6624, Faculté des Sciences, La Bouloie, Université de Franche-Comté,  
 25030 Besançon Cedex, France*

(Received 2 December 1999)

The structure and lattice dynamics of a physisorbed acetylene monolayer on a KCl(001) single crystal surface have been investigated by comparing helium atom scattering experiments with calculations based on a semi-empirical potential. A  $(\sqrt{2} \times \sqrt{2})R45^\circ$  structure is determined from diffraction measurements. The time of flight spectra reveal at least three well separated adsorbate layer phonon modes along the [110] direction, two of which are only weakly dispersive, while the third is characterized by a very pronounced dispersion. The calculations also predict a  $(\sqrt{2} \times \sqrt{2})R45^\circ$  structure containing two molecules per unit cell, which lie flat on the surface and which are mutually perpendicular. The phonons calculated for this structure are used to assign the observed dispersion curves.

### I. INTRODUCTION

Multipolar molecules physisorbed on ionic single-crystal surfaces exhibit a wealth of low and high order commensurate structures, which have been widely studied over the last decade both experimentally<sup>1-8</sup> and theoretically.<sup>9-17</sup> Indeed multipolar molecules tend to arrange themselves on a surface according to their own translational and orientational geometries consistent with minimum lateral interactions. Yet, large electric fields are generally present at the surface of ionic crystals that are responsible for large corrugations and thus for adsorption sites with deep wells. As a result of the competition between the binding and lateral interactions, various commensurate structures occur, depending on the ability of the molecules to arrange their centers of mass and their axes in ordered geometries consistent with the substrate periodicity. Low energy electron diffraction<sup>5,8</sup> (LEED) and helium atom scattering<sup>2,7</sup> (HAS) diffraction experiments provide information on the translational geometry of the adsorbate, whereas polarization infrared spectroscopy<sup>1,3,4,6</sup> (PIRS) is sensitive to the orientation of the ad molecules. The dynamics of the collective adlayer motions is best determined from inelastic time-of-flight (TOF) helium atom scattering data, since electron energy loss spectroscopy (EELS) may lead to damage and special precautions are needed to avoid structural changes. For interpreting the data *ab initio* potential energy calculations<sup>15,16</sup> have proven to be useful in determining the adsorbate geometries, although they are very time consuming and then often limited to small systems. In contrast, semiempirical potentials are suitable for systems with a large number of degrees of freedom,<sup>10,12</sup> and, due to their relative simplicity, they can be used to simulate dynamical processes with molecular dynamics calculations.<sup>9,17</sup>

The complementarity of experimental and theoretical approaches for obtaining a detailed picture of adsorbate geometry and dynamics was illustrated in previous collaborative studies on the systems CO/MgO,<sup>18,19</sup> OCS/NaCl,<sup>20</sup> and the C<sub>2</sub>H<sub>2</sub>/NaCl system.<sup>7,21</sup> For the latter system HAS

experiments<sup>7</sup> showed the existence of two C<sub>2</sub>H<sub>2</sub> monolayer phases, depending upon the coverage and temperature. At  $T=90$  K, a stable low-density phase containing four molecules in a rotated  $(3\sqrt{2} \times \sqrt{2})R45^\circ$  unit mesh was observed, whereas at  $T=80$  K, the adsorbate growth continued up to the formation of a higher-density phase, with a  $(7\sqrt{2} \times \sqrt{2})R45^\circ$  unit cell, containing seven molecules. This latter phase, which was attributed to the complete monolayer, was characterized by a buckling due to the large misfit of about 8% between the bulk acetylene lattice constants<sup>22,23</sup> and the Na-Na distance ( $a_s=3.96$  Å). Theoretical studies based on both *ab initio*<sup>15</sup> and semiempirical<sup>21</sup> potentials showed that the acetylene molecules were adsorbed parallel to the surface in the two phases, in agreement with the assignment deduced from the measurement of the intensity ratios of the polarized infrared bands. Inelastic HAS experiments performed on the low density phase<sup>21</sup> revealed two nondispersive Einstein modes at around 8.2 and 14.5 meV, which were attributed, on the basis of the theoretical study of the phonon-libron modes, to the perpendicular vibrations of the centers of mass and to angular librations (tumbling mode) of the molecular axes, respectively. By contrast the HAS experiments failed in giving resolvable TOF spectra for the dynamics of the high-density phase, possibly due to the buckling phenomenon.

In the present work, the structure and the dynamics of acetylene layers adsorbed on the KCl(001) substrate have been studied using both elastic and inelastic TOF helium scattering. KCl was chosen, because its larger unit cell<sup>22</sup> ( $a_s=4.38$  Å) is in better registry with the lattice parameter of acetylene than for NaCl. This should favor the formation of a full monolayer without any buckling and also favor layer-by-layer growth. Molecular dynamics simulations based on semiempirical potentials are used to determine the equilibrium structure of the first layer of C<sub>2</sub>H<sub>2</sub> at  $T=0$  K. For the calculations of the phonons and librons of the acetylene monolayer the same formalism is used as previously

applied to the  $C_2H_2/NaCl$  system.<sup>21</sup>

The present paper is organized as follows. The experimental setup and data analysis are presented in Secs. II and III. In Sec. IV the details of the calculational procedure of the monolayer structure and the dynamics are given and followed by the presentation of the theoretical results in Sec. V. In Sec. VI, the theoretical results are compared to the experimental data and with the previous analysis of the  $C_2H_2/NaCl$  system. Final concluding remarks follow in Sec. VII.

## II. EXPERIMENT

The experimental apparatus is described in detail elsewhere.<sup>24</sup> A nearly monoenergetic He atom beam (FWHM) [full width at half maximum of  $\Delta v/v \sim 1\%$ ;  $\Delta E/E \sim 2\%$ ] is generated by continuous expansion of He gas through a nozzle of  $10 \mu\text{m}$  in diameter from a stagnation pressure of 50–100 bar. Incident beam energies in the range of 15.0–21.5 meV are achieved by varying the source temperature between 70 and 100 K, respectively. The angle between incident and final scattered beams is  $90^\circ$ , thus the incident  $\theta_i$  and final  $\theta_f$  angles measured with respect to the surface normally obey the relationship  $\theta_i + \theta_f = 90^\circ$ . After scattering from the crystal surface the He atoms are detected by a magnetic mass spectrometer at the end of a 1.4 m long time-of-flight tube. Angular distributions are measured with a continuous beam by rotating the crystal around an axis perpendicular to the scattering plane and hence varying incident and final angles simultaneously. The parallel wave vector change is given by  $\Delta K = k_f \sin \theta_f - k_i \sin \theta_i$ , where  $k_i$  and  $k_f$  are the incident and final wave vectors.

The KCl surface was prepared by cleaving off a small slice from a KCl single crystal with  $10 \times 10 \text{ mm}^2$  surface area at a surface temperature of 100 K under UHV conditions in the  $10^{-11}$  mbar range. After cleavage and between measurements the crystal was heated up to 400 K to prevent possible deterioration of surface quality by residual water. The acetylene gas (Messer-Griesheim GmbH, purity 99.6 % with the main impurity being acetone) was purified in 5–6 cycles of condensing the acetylene in a liquid- $N_2$  trap, pumping the gas line to remove volatile impurities like hydrogen, and again warming up the cold trap. During gas dosage the acetone was frozen out in a cold trap filled with a mixture of *n*-pentane and liquid  $N_2$  at 223 K.

## III. EXPERIMENTAL RESULTS

The monolayers of acetylene on KCl were prepared by applying a constant  $C_2H_2$  background pressure of  $5 \times 10^{-8}$  mbar through an UHV leak valve at a constant crystal temperature of  $T_s = 75$  K. Simultaneously the specular intensity was monitored as shown in Fig. 1. Following an initial steep decline, after 15 minutes, corresponding to an exposure of 45 L (1 L = 1 langmuir =  $10^6$  Torr s), the intensity of the specularly reflected He beam became constant, indicating that a stable phase, which is assigned to the first monolayer, had been formed. At 75 K the monolayer phase was stable without further dosage of acetylene and stayed sufficiently clean for at least 10 h. Careful investigation of the specular intensity during cooling of the crystal at con-

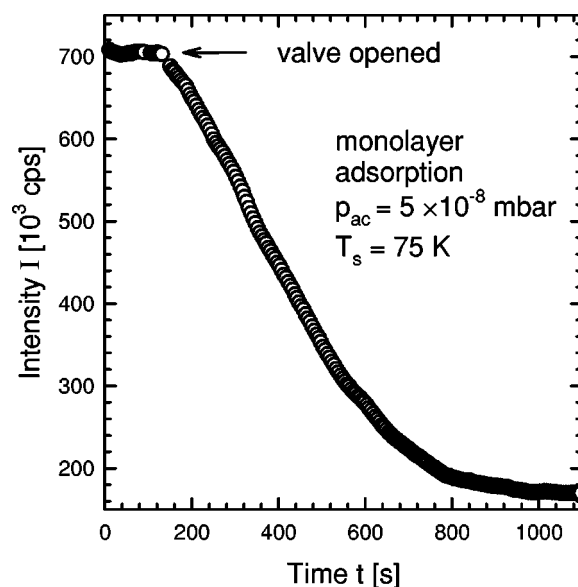


FIG. 1. Specular He signal measured with an incident wave vector of the He beam of  $4.9 \text{ \AA}^{-1}$  during the adsorption of a monolayer of  $C_2H_2$  on  $KCl(001)[110]$  at a surface temperature of 75 K and an acetylene partial pressure of  $5 \times 10^{-8}$  mbar. At these conditions no further adsorption was observed.

stant exposure to  $5 \times 10^{-8}$  mbar of  $C_2H_2$  showed that this phase exists at least down to a temperature of about 70 K at which three-dimensional (3D) condensation starts and to above 93 K where the adlayer desorbs without additional gas exposure. Thus, different from the adsorbate  $C_2H_2/NaCl(001)$ , where two phases were found as a function of coverage and temperature, in the system  $C_2H_2/KCl(001)$  apparently only one phase is formed. However, the latter is not unexpected due to the significantly better lattice matching, as discussed in Sec. I.

A monotonous decrease of the specular intensity upon exposure of the surface to the adsorbing species has been observed before for, e.g.,  $CO_2/NaCl(001)$  (Ref. 25) and  $CH_4/NaCl(001)$  (Ref. 26). It is indicative of the growth of the monolayer in large islands and clearly distinguishes the growth mechanism from filling the monolayer via a lattice gas, where a pronounced minimum of the specular intensity is to be expected. The latter was found for the monolayer  $CO/NaCl(001)$ .<sup>27</sup> From the experimentally determined desorption temperatures of 90–93 K the heat of desorption of  $C_2H_2/KCl(001)$ , which is assumed to be close to the adsorption energy, was estimated to  $-27 \pm 1$  kJ/mol ( $-280 \pm 10$  meV per molecule).

In order to determine the structure of the monolayer, diffraction scans were taken along the [100], [110], [210], and [310] surface azimuths at an incident beam energy of 21.4 meV. Figure 2 shows diffraction patterns of the substrate (left) and the monolayer (right) along the first three directions (along the fourth no additional features were observed, which excludes a higher superstructure than that discussed below). The figure also shows the position of the diffraction peaks in the reciprocal lattice. Half-ordered diffraction peaks are only visible in the [210] direction. From the diffraction pattern a  $(\sqrt{2} \times \sqrt{2})R45^\circ$  superstructure can be unambiguously concluded. The absence of half-order features along the [100] azimuths indicates the existence of glide planes

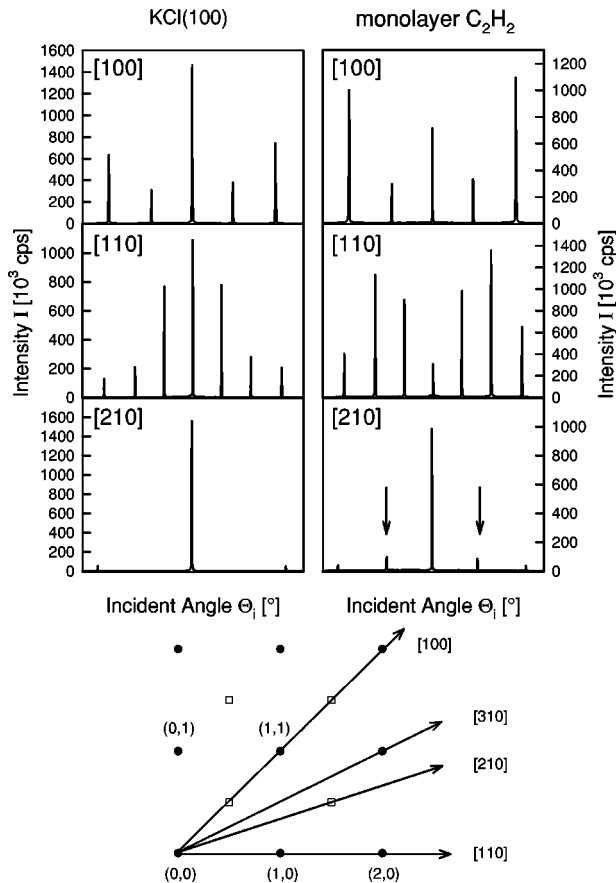


FIG. 2. Diffraction scans along the  $[100]$ ,  $[110]$ , and  $[210]$  crystal directions for the KCl(001) surface (left) and the monolayer of  $C_2H_2$  (right) measured with a wave vector of the incident He beam of  $6.4 \text{ \AA}^{-1}$ . Only along the  $[210]$  direction superstructure peaks have been observed (marked with arrows). The lower part depicts the measured azimuthal directions and the reciprocal lattice of the  $(\sqrt{2} \times \sqrt{2})R45^\circ$  structure, open squares representing the half-ordered peaks. The missing half-order spots along the  $[100]$  direction is indicative of glide planes along the borders of the adsorbate lattice unit cell.

along these directions in the adsorbate lattice unit cell.

A total of 40 TOF spectra of the monolayer were measured along the  $[110]$  direction at an incident beam energy of 19.2 meV and a sample temperature of  $T_s = 75 \text{ K}$ , without further exposure to acetylene. Under these surface conditions further adsorption could be excluded. For a single TOF spectrum data were accumulated for about 35 min and after each 9 h the monolayer was desorbed and freshly prepared. Figure 3(a) shows examples for TOF spectra at incident angles of  $36.5^\circ$ ,  $42.5^\circ$ , and  $52.5^\circ$ . In Fig. 3(b) the corresponding scan curves, which correlate energy and momentum conservation for the respective angle of incidence in the  $\Delta E$  vs  $\Delta K$  diagram, as well as the phonon features from all TOF spectra are shown. An easier interpretation of these data is possible after folding them back into the first Brillouin zone [see Fig. 3(b)].

The experimental error in determining each data point results from the energy spread of that special peak that leads to an uncertainty in both the energy transfer and the parallel momentum transfer calculated from the scan curves. The estimated corresponding error differs strongly within the pa-

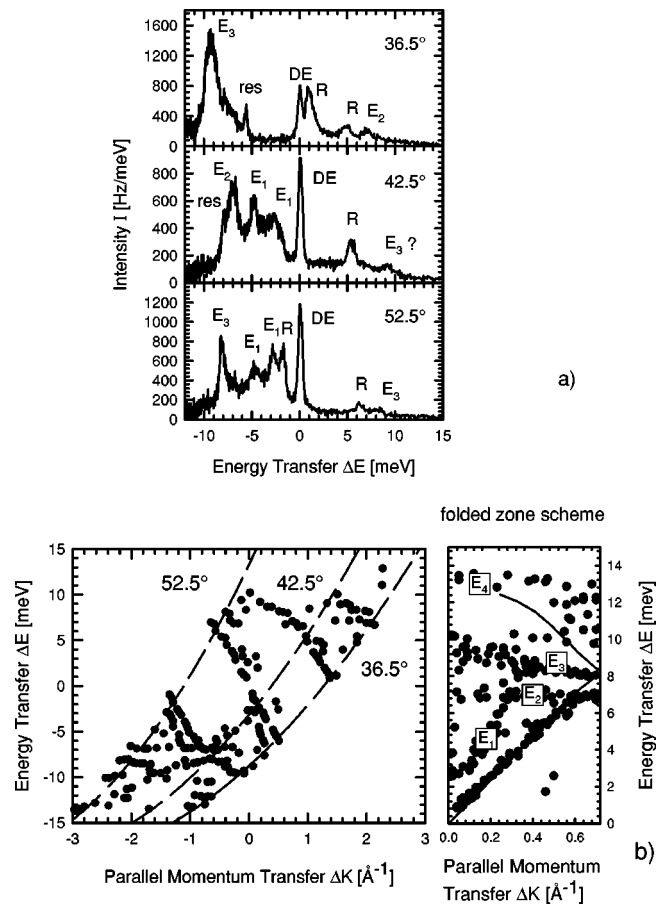


FIG. 3. Examples of (a) TOF spectra of the monolayer  $C_2H_2$  on KCl(001) measured at incident angles of  $36.5^\circ$ ,  $42.5^\circ$ , and  $52.5^\circ$  along the  $[110]$  crystal direction, at an incident beam energy of 19.2 meV and a surface temperature of 75 K. The monolayer modes are assigned with an E. In addition, the diffuse elastic peak, DE, the Rayleigh mode of the substrate, R, are visible as well as some sharp features, “res”, which could be assigned to selective adsorption resonances. In the lower panel (b) the complete dispersion curve is shown together with the three scan curves, along which the spectra in (a) were measured. Also shown is a dispersion diagram that has been folded back into the positive energy, positive momentum transfer region of the first Brillouin zone. Phonons measurable on the bare KCl(001) substrate are marked by solid lines.

rameter range of this experiment, but is in any case within the size of the symbols used in Fig. 3(b), left panel. In addition, there may also be small systematic errors in the measurement of the time of flight and the scattering angles. Because of the calibrations and extensive past experience<sup>24</sup> they are estimated to be also of the same size.

For comparison, dispersion curves of the pure KCl surface were also measured along this direction, and found to agree with earlier HAS measurements.<sup>28</sup> The bare surface is characterized by a Rayleigh mode with an energy of 8.5 meV at the zone boundary and by a folded mode, which is due to the similarity of the masses of the potassium and chloride ions. These KCl modes are also shown in Fig. 3(b) as solid lines. In addition, some peaks of less intensity, which have been assigned to an optical mode above 15 meV, were also observed.

In the adsorbate dispersion diagram at least three phonon modes are observed, which are not found on the bare

KCl(001) surface. The Rayleigh mode  $R$  of the substrate is visible up to a parallel momentum transfer of  $0.6 \text{ \AA}^{-1}$ , where it intersects a nearly dispersionless adsorbate mode at 7 meV, which is denoted as  $E_2$  in Fig. 3. Another only weakly dispersive mode ( $E_3$ ) is found with an energy of about 8 meV at the zone boundary. It seems to have about 10–15 % larger energy at the zone center. However, the scatter of the data for small parallel momentum transfers may suggest that in this regime they are due to more than only a single mode. Additionally, the monolayer shows a strongly dispersive mode ( $E_1$ ) starting at 2.8 meV at the  $\Gamma$  point, i.e., the zone center. Its energy increases by more than a factor of 2 within the first 40% of the Brillouin zone, after which it cannot unambiguously be followed. In addition, at a beam energy of 19.2 meV at least two more weakly dispersive modes seem to be observable with energies of about 13 and 10 meV, respectively. The latter was seen in the outer part of the Brillouin zone only. The former will be denoted as  $E_4$ .

An intensity analysis of the observed phonons shows that mode  $E_1$  decreases from the zone center towards the border, which indicates a significant contribution of motions perpendicular to the surface. In contrast, the intensity of the almost dispersion-free mode  $E_2$  increases towards the zone boundary, which suggests significant contributions parallel to the surface. The intensity analysis for modes  $E_3$  and  $E_4$  gives no unambiguous results.

Measurements were also performed along the [100] crystal direction. They revealed at least three modes, which are with respect to the energetic positions and the forms of the dispersion curves very similar to the modes  $E_1$ – $E_3$  along the [110] direction.

## IV. THEORETICAL CALCULATIONS

### A. Potential energy

As in the previous study of  $C_2H_2$  on  $NaCl$ ,<sup>21</sup> both the acetylene molecule and the KCl substrate are assumed to be rigid, and the total interaction potential is separated into a sum of molecule-substrate ( $V^{MS}$ ) and lateral molecule-molecule ( $V^{MM}$ ) potential terms. Each of these potentials consists of electrostatic, dispersion-repulsion, and induction contributions.

The electrostatic contribution of  $V^{MS}$  accounts for the interaction between the charges  $\pm e$  ( $e$  is the electron charge) of the substrate ions and the electric multipoles of the admolecule, whereas the corresponding contribution in  $V^{MM}$  considers interactions between multipole moments belonging to different admolecules. The charge distribution of the acetylene molecule can be mimicked by either a single point quadrupole moment equal to  $7.2 D\text{\AA}$  ( $=5.355 \text{ a.u.} = 2.4 \cdot 10^{-39} \text{ Cm}^2$ ) located at the center of mass<sup>29</sup> or by a set of multipoles, up to the hexadecapole moment, localized on the C and H atoms, which accounts for the nonlocal electronic extension of the molecule [distributed multipole analysis (DMA) approach].<sup>30–32</sup> The values of the multipoles are those given in Ref. 21. The effect of the two descriptions (point and distributed approaches) on the adsorption properties of  $C_2H_2$  will be discussed later in the paper.

The dispersion-repulsion interactions in  $V^{MS}$  and  $V^{MM}$  are described by site-site pairwise Lennard-Jones potentials where the sites are the C, H, K, and Cl nuclei. The values of

the parameters  $\epsilon$  and  $\sigma$  for C and H are taken from Ref. 21, and those for K and Cl are from an analysis of ion-water microcluster structures.<sup>33</sup> The  $\sigma$  parameters for the pair interactions between KCl and  $C_2H_2$  were slightly adjusted by 10% in order to fit the experimental value of the isosteric heat of adsorption of  $C_2H_2$  on KCl. This fit did not influence the equilibrium geometry of the admolecules. The induction terms that describe the mutual polarization of the substrate and of the admolecules are less than 10–15 % of the other contributions.

The total interaction potential between the  $C_2H_2$  admolecules and the KCl substrate is then written as

$$V = \sum_i \left[ \sum_{l,s,p} V^{MS}(\mathbf{r}_{ilsp}, \boldsymbol{\Omega}_i) + \sum_{j \neq i} V^{MM}(\mathbf{r}_{ij}, \boldsymbol{\Omega}_i, \boldsymbol{\Omega}_j) \right], \quad (1)$$

where  $\mathbf{r}_{ilsp}$  is the distance between the center of mass of the molecule  $i$  and a substrate atom  $s$  of the  $l$ th unit cell in a plane  $p$  of the substrate, and  $\mathbf{r}_{ij}$  is the distance between two atoms belonging to the  $i$ th and  $j$ th molecules.  $\boldsymbol{\Omega}_i$  describes the orientation of the  $i$ th acetylene molecule in the coordinate system of the surface.

### B. Monolayer structure

To determine the equilibrium structure of the adsorbate, the potential  $V$  [Eq. (1)] was minimized with respect to the positions  $\mathbf{r}_i = (x_i, y_i, z_i)$  and orientations  $\boldsymbol{\Omega}_i = (\theta_i, \phi_i)$  of the admolecules, using a conjugate gradient method.<sup>34</sup> The potential energy surface of a single admolecule obtained from a  $(x, y)$  sampling of points above the surface provides the important properties such as the stable site, saddle point, and potential corrugation. Based on experimental results, only a selection of the infinite number of possible adsorbate structures was investigated. Various  $(m\sqrt{2} \times n\sqrt{2})R45^\circ$  commensurate structures were considered for the monolayer, where  $m$  and  $n$  are integers. Since the misfit between the bulk parameter of acetylene and the lattice parameter of KCl ( $a_s = 4.38 \text{ \AA}$ ) is less than 2%,<sup>22</sup> only values of  $m \leq 2$  and  $n \leq 2$  were chosen. The molecule density of these phases corresponds to the completion, i.e., one molecule per substrate cation site. The monolayer structure was obtained from a numerical search for the potential minimum with respect to the  $2 \times m \times n \times 5$  variables in the cells of the different phases investigated. To avoid secondary minima, the minimization was carried out for a large number of initial configurations (about  $10^3$ ), making the numerical search for the minimum energy structure time consuming. For the monolayer, the smallest unit cell consistent with attractive lateral interactions is found to be the  $(\sqrt{2} \times \sqrt{2})R45^\circ$  cell containing two molecules, in agreement with the experiment.

### C. Monolayer dynamics

Once the stable structure is known, the monolayer translation-orientation dynamics and the dispersion curves can be calculated. The harmonic dynamical matrix of the monolayer is a  $(5N_s \times 5N_s)$  rank square matrix (where  $N_s$  is the number of molecules per monolayer unit cell) defined by its components<sup>21</sup>

$$\begin{aligned}
D_{\alpha,\alpha'}(m,m',\mathbf{q}) = & \sum_{r'} \frac{1}{\sqrt{A_\alpha A_{\alpha'}}} \left[ \phi_{\alpha,\alpha'}^{MM}(r,m,r',m') \right. \\
& \left. + \sum_{l,s,p} \phi_{\alpha,\alpha'}^{MS}(r,m,l,s,p) \delta_{r,r'} \delta_{m,m'} \right] \\
& \times e^{-i\mathbf{q}\cdot[\mathbf{R}(r)-\mathbf{R}(r')]}, \quad (2)
\end{aligned}$$

where  $A_\alpha$  is either the effective molecular mass  $A = 4.32 \times 10^{-23}$  g molecule $^{-1}$  for the translational coordinates  $\alpha = x, y$ , and  $z$ , or the moment of inertia  $I$  or  $I \sin^2 \theta$  ( $I = 23.78 \times 10^{-40}$  g cm $^2$  molecule $^{-1}$ ) for the angular variables  $\alpha = \theta$  or  $\phi$ . These latter variables define the polar and azimuthal angles of the molecular axis with respect to an absolute frame tied to the surface (where the  $z$  axis is along the normal to the surface). The lateral force constant tensor  $\phi^{MM}$  correlates the motions of two acetylene molecules and  $\phi^{MS}$  characterizes the force constant tensor between an ad-molecule and the static substrate.  $\mathbf{R}$  denotes the equilibrium position of the  $r$ th unit cell of the layer with respect to the origin and  $\mathbf{q}$  is the two-dimensional wave vector in the  $(x, y)$  surface plane. The diagonalization of  $\underline{D}$  provides a set of  $5N_s$  eigenvalues  $\omega_\lambda(\mathbf{q})$ , which are the frequencies of the phonons and librations for each  $\mathbf{q}$  value. From the eigenvectors  $\mathbf{e}(m, \mathbf{q}, \lambda)$  of  $\underline{D}$  the spectral density associated with the corresponding dispersion curves<sup>35</sup> is calculated:

$$\rho_\alpha(\omega) = \sum_{\lambda, m, \mathbf{q}} |e_\alpha(m, \mathbf{q}, \lambda)|^2 \delta(\omega - \omega_\lambda(\mathbf{q})). \quad (3)$$

This quantity provides the polarization of the various external modes of the monolayer.

#### D. Molecular dynamics simulations

Finite temperature molecular dynamics simulations were used to determine the structure of the adsorbate above  $T=0$  K, which is out of the minimization procedure capability. The acetylene molecules were initially placed and oriented at their minimum energy configuration obtained from the  $T=0$  K minimization. 64 molecules, i.e., one molecule per cation site, were placed on a patch of  $8 \times 8$  unit cells of the substrate. This patch was periodically replicated along the surface plane, and a reflection barrier 30 Å above the surface prevented desorption of the molecules during the simulation.

In the molecular dynamics calculations, the rotational equations of motion were solved by a leap-frog algorithm based on a quaternion representation of the molecular orientations, and a leap-frog extension to the method of Verlet was used for the translation equations of motion.<sup>36</sup> A time step of 3.0 fs was considered. After equilibration over 12 000 steps (corresponding to a real time of 36 ps), data were collected for the next 6000 steps (18 ps). The initial linear and angular velocities were taken from a Boltzmann distribution corresponding to the desired simulation temperatures consistent with experiments, namely 40 and 75 K. The temperature was held constant during the production run by scaling the velocities every 20 steps. Tests showed that the results ob-

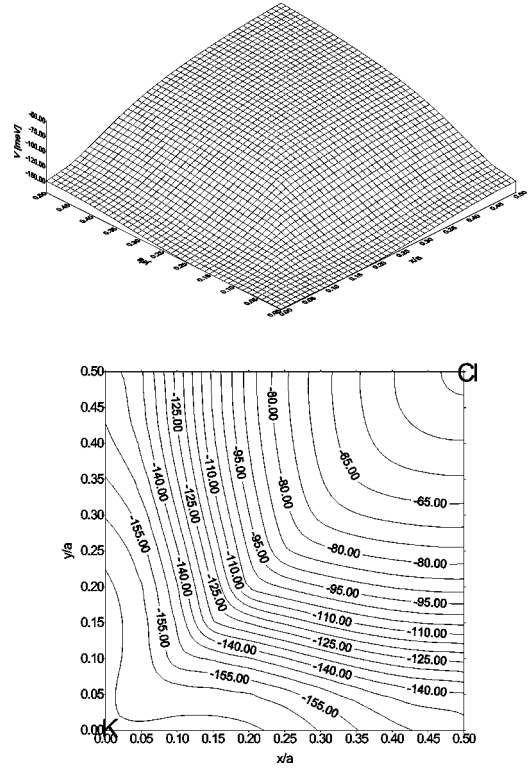


FIG. 4. Potential energy surface experienced by a single  $\text{C}_2\text{H}_2$  ad-molecule above KCl (point quadrupole model). The origin ( $x=0, y=0$ ) corresponds to a cation site, whereas ( $x/a=0.5, y=0$ ) ( $a=4.38$  Å) defines the site between two consecutive cations. Energy in meV and distances in reduced units of  $a=4.38$  Å.

tained with this rescaling procedure were not significantly different from runs done within the microcanonical ensemble.<sup>37</sup>

The energy, forces, and torques were calculated within the point quadrupole description for acetylene, only. Indeed, the distributed multipole approach leads to an unrealistic divergence in the force constant calculations when two multipolar sites tend to be too close to each other. For the interactions within the monolayer a radial cutoff of 17 Å was used and the calculations in the reciprocal space of the substrate were carried out for the binding potential. Calculations of the lateral interactions within the adlayer were speeded up by using a neighbor list.<sup>36</sup>

## V. THEORETICAL RESULTS

### A. Monolayer structure

Figure 4 shows the potential energy surface (PES) for a single  $\text{C}_2\text{H}_2$  molecule adsorbed on KCl(001) using the point multipole electrostatic model. Since the PES obtained with the distributed multipole approach has a similar shape, it is not shown. The most stable adsorption site is above the cation, where the molecule lies flat ( $\theta=90^\circ$ ) at a distance  $z=3.35$  Å from the surface ( $z=3.44$  Å with the DMA model). The molecular axis is parallel to a cation row in the point model, whereas the positive charges on the hydrogen atoms favor a preferential interaction with the  $\text{Cl}^-$  anion, leading to a molecular axis orientation along the K-Cl direction, in the distributed approach. The potential well depth in

the stable adsorption site in the point description is equal to 167 meV compared to 146 meV with the DMA model. Above the anion, the molecular axis is perpendicular to the surface and the molecule is less bound to the surface by about 50 meV. Note finally that the PES is flat around the cation site, and that the corrugation remains small along the cation rows (20 meV for the two models), with a saddle point at the middle of the distance between two adjacent K atoms.

In the most stable geometry ( $\sqrt{2} \times \sqrt{2}$ ) $R45^\circ$ , the two molecules have different orientations in the unit cell. The molecular centers of mass are located on two adjacent cation sites, at the same molecule-surface distance which is close to the single molecule value ( $z=3.37$  Å with the point model and  $z=3.43$  Å in the distributed approach). The molecular axes lie parallel to the surface, but the two molecules in the unit cell are perpendicularly oriented to minimize the lateral interactions. The molecules in the unit cell are related to each other by two glide planes along the  $\langle 100 \rangle$  and the  $\langle 010 \rangle$  directions. The mean energy per molecule is equal to  $-324$  meV and the lateral and the molecule-surface interactions contribute in a similar way since  $V^{MS}/V^{MM}=1.04$  for the point model. When the DMA is used, the mean energy is  $-310$  meV, and the ratio  $V^{MS}/V^{MM}$  becomes slightly smaller (0.81). This geometry is very stable since, in the minimization procedure, the nearest local minimum had a significantly larger energy of about 50 meV. In this case the molecular axes also lie parallel to the surface, but are mutually parallel. Upon increasing  $m$  and  $n$  the geometries remain unchanged since the most stable phases with  $m > 1$  and/or  $n > 1$  obtained from the minimization procedure correspond to juxtapositions of ( $\sqrt{2} \times \sqrt{2}$ ) $R45^\circ$  unit cells.

Molecular dynamics simulations of the acetylene monolayer adsorbed on KCl were performed for two different temperatures, namely 40 and 75 K, in accordance with experiments. At  $T=40$  K, the distribution function  $p(z)$  of the distance between the molecular center of mass and the surface exhibits a single sharp peak at  $z=3.38$  Å. This peak does not shift significantly with increasing temperature [Fig. 5(a)], but it broadens slightly as a result of large amplitude translational motions. The distribution functions  $p(\theta)$  and  $p(\phi)$  [Figs. 5(b) and 5(c)] show a single peak at  $\theta=90^\circ$  and two peaks at  $\phi=0^\circ$  and  $90^\circ$ , respectively, which are not significantly modified when  $T$  increases from 40 to 75 K. At both temperatures the molecules have the same ( $\sqrt{2} \times \sqrt{2}$ ) $R45^\circ$  structure as in the 0 K calculation. A snapshot at an intermediate stage in the simulations at 75 K shown in Fig. 6 illustrates the approach to the final structure. The average total energy per molecule increases from  $-306$  to  $-291$  meV when the temperature increases from 40 to 75 K. Note that the ratio of the lateral and molecule-surface interactions remains very close to the one determined in 0 K calculations (1.04 at 40 K and 1.02 at 75 K).

### B. Monolayer phonon-libron dispersion curves

Only the point interaction model was used for the calculation of the phonon-libron dynamics of the acetylene monolayer because, as already mentioned, the distributed model leads to artifacts in the force constants. Similar problems have been discussed by Gamba and Bonadeo,<sup>38</sup> who showed

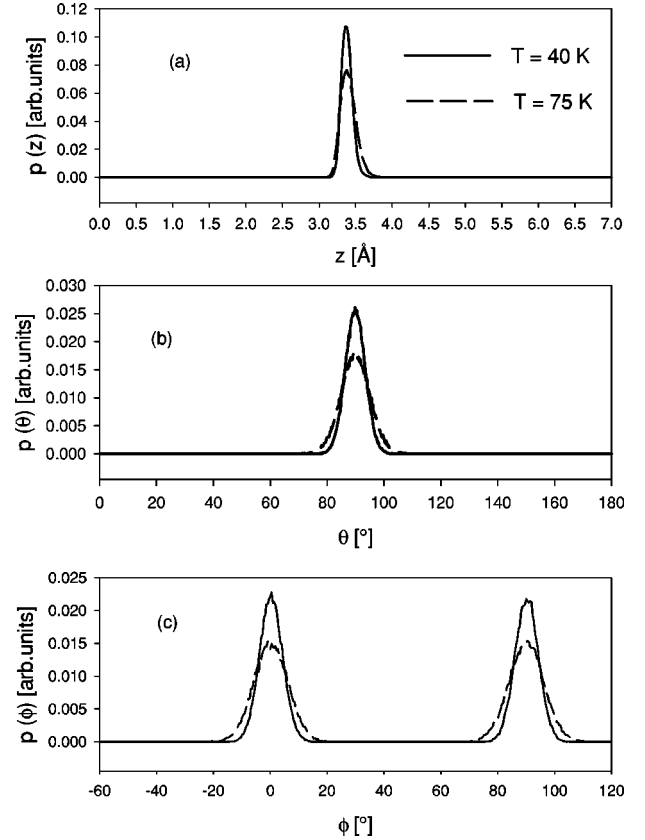


FIG. 5. Results of the simulation for the  $C_2H_2$  monolayer adsorbed on KCl at  $T=40$  and 75 K. (a) Distribution function  $p(z)$  in arbitrary units (arb. units) of the molecule-surface distance  $z$  (in Å). (b) Distribution functions (in arb. units)  $p(\theta)$  of the polar angle  $\theta$  and  $p(\phi)$  of the azimuthal angle  $\phi$ .

that the distribution of multipoles on different sites of the acetylene molecule generally leads to some imaginary frequencies in the lattice dynamics of the bulk crystal, unless up to the  $2^6$ -poles are taken into account.

Figure 7 exhibits the dispersion curves for the translational and orientational dynamics of the ( $\sqrt{2} \times \sqrt{2}$ ) $R45^\circ$   $C_2H_2$  monolayer along the  $[110]$  direction. In principle, the solution for a dynamical matrix  $D$  of rank 10 leads to ten dispersion curves with  $q$  in the range  $0$  to  $\pi/(a_s\sqrt{2})$ , where  $a_s$  is the substrate parameter. Due to the symmetry of the surface, two domains with perpendicular unit cells can exist on the surface. However, since the surroundings in the two domains are identical, the corresponding dispersion curves are degenerate. Their energies range between 2 and 16 meV. The acoustic branches of the bare KCl substrate including the Rayleigh mode as well as the experimentally determined phonon data are also depicted in Fig. 7.

The dynamical coupling in the adsorbate leads to hybridizations of the molecular motions and therefore no strictly pure modes are observed in the calculations. The strongly dispersive quasi-acoustic mode  $A_1$  with an energy equal to 2.5 meV at the  $\Gamma$  point of the first Brillouin zone (FBZ) corresponds mainly to parallel ( $x, y$ ) translational motions of the molecular centers of mass with, however, a significant hybridization with the perpendicular ( $z$ ) translation. At the end of the FBZ, this mode is fully polarized perpendicular to

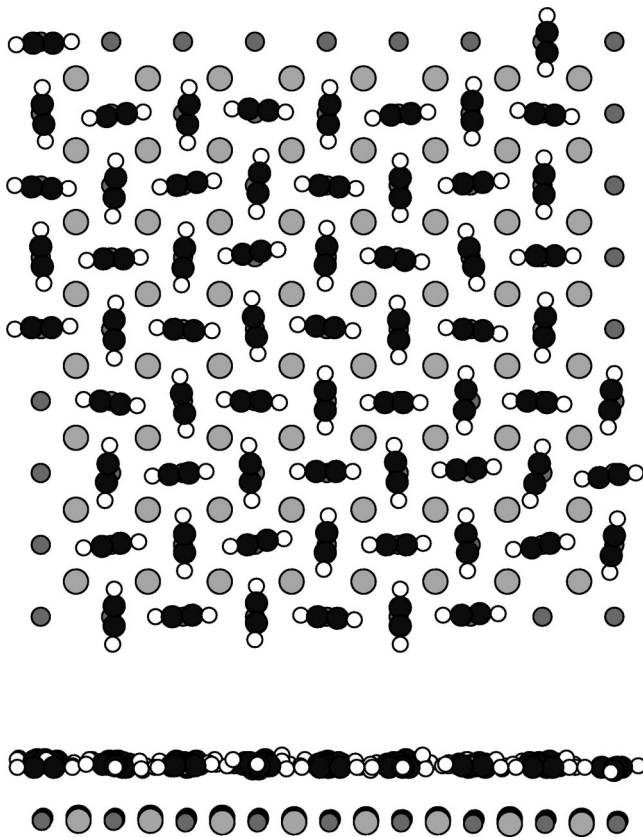


FIG. 6. Top and side views of a snapshot of the simulation of the acetylene monolayer on KCl at  $T=75$  K. Small and large gray circles represent K and Cl sites, respectively. Black and white circles correspond to the C and H atoms, respectively.

the surface and characterizes the  $z$  motion, only. The energy gap of 2.5 meV characterizes the substrate corrugation experienced by the admolecule, as shown in the PES of Fig. 4. The much less dispersive mode  $A_2$  around 6.5 meV describes mainly translational motions perpendicular to the surface. Modes  $A_3$ ,  $A_4$ ,  $A_5$ , and  $A_6$  with energies ranging between 8 and 12 meV are clearly related to the  $x$  and  $y$  translations and are polarized parallel to the surface. The nondispersive modes  $A_7$  and  $A_8$  around 13 meV are characterized by  $\theta$  angular motions perpendicular to the surface. The higher-energy branches  $A_9$  and  $A_{10}$  at around 16 meV correspond to  $\phi$  azimuthal librations of the molecular axes in a plane parallel to the surface. The right hand side of Fig. 7 shows the corresponding spectral densities for polarizations parallel and perpendicular to the surface [Eq. (3)]. These curves do not show any signal below 6 meV due to the dispersive behavior of the phonon branches. The first intense peak occurs at around 6.5 meV with the perpendicular polarization which characterizes the  $A_1$  mode at the end of the FBZ and the undispersive mode  $A_2$ . The other peaks corresponding to  $\rho_{\perp}$  are the  $\theta$  librational modes around 13 meV. The parallel motions give rise to three structures in  $\rho_{\parallel}$ , two sharp peaks being connected to  $A_4$  and ( $A_5$ ,  $A_6$ ) branches, and a broad signal being attributed to  $A_9$  and  $A_{10}$ .

## VI. DISCUSSION AND COMPARISON WITH THE EXPERIMENTS

The interaction of a single admolecule with the KCl substrate favors a stable adsorption site above the cation, with an

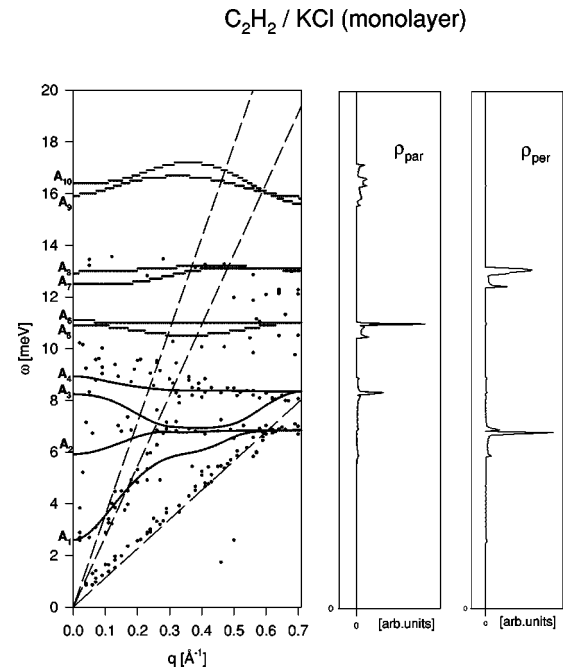


FIG. 7. Dispersion curves for the  $C_2H_2$  monolayer adsorbed on KCl(001) ( $q \equiv \Delta K$ ). Full curves represent calculations while points correspond to the experimental data. The acoustic modes of the bulk substrate are represented by dashed lines (the lowest-energy mode corresponds to the Rayleigh mode). The experimental error is smaller than 0.7 meV and  $0.1 \text{ \AA}^{-1}$ . The calculated parallel and perpendicular spectral densities of phonon state are given in arbitrary units (arb. units) at the right hand side of the figure.

orientation of the molecular axis parallel to the surface. Such a geometry, for which at present there is no direct experimental evidence, is very similar to that obtained for acetylene adsorbed on NaCl and was corroborated by periodic Hartree-Fock calculations.<sup>15</sup> The molecule-substrate binding energy is for KCl equal to 167 meV or to 146 meV, depending on the potential model used (point quadrupole or DMA, respectively) and is slightly smaller than for the NaCl substrate (198 meV).<sup>21</sup> This decrease is due to the larger substrate unit cell parameter for KCl, and thus to a smaller ion surface density, which is responsible for a smaller electric field at the KCl surface.

The 0 K minimization procedure of the monolayer-substrate interactions leads to the most stable  $(\sqrt{2} \times \sqrt{2})R45^\circ$  phase containing two molecules per unit cell related by two glide planes. This configuration corresponds to the monolayer completion with one acetylene molecule per substrate cation. In the point quadrupole description, the molecules are adsorbed parallel to the substrate along the K rows with their axes mutually perpendicular, and the corresponding energy per molecule is twice the single admolecule adsorption energy, indicating that lateral and molecule-surface interactions contribute nearly equally. Molecular dynamics simulations at finite temperature (up to 75 K) show that the 0 K structure is very stable, the energy per molecule being slightly higher ( $-306$  meV at 40 K, and  $-291$  meV at 75 K) due to the kinetic contribution equal to about 9 meV at 40 K and 16 meV at 75 K. These results are fully consistent with the HAS data regarding the  $(\sqrt{2} \times \sqrt{2})R45^\circ$  geometry of the acetylene monolayer, as well

as the value of the heat of adsorption equal to  $-27 \pm 1$  kJ/mol ( $-280 \pm 10$  meV per molecule) as determined from desorption temperatures.

The calculated extrinsic vibrations of the monolayer can be compared directly with results from the present inelastic helium atom time-of-flight spectroscopy. The experimental dispersion curves show the existence of a strong acoustical mode ( $E_1$ ) starting at 2.8 meV and of two nearly dispersionless modes around 7 meV ( $E_2$ ) and between 8 and 9 meV ( $E_3$ ). An additional optical mode is also visible in the range 12–13 meV ( $E_4$ ). In the comparison between the calculated phonon modes and the corresponding experimental data displayed in Fig. 7, the calculated high-frequency modes  $A_9$  and  $A_{10}$ , which correspond primarily to  $\phi$  angular motions, are not observed. This is due to the relatively low incident energy of the helium atoms (19.2 meV), which is too low to excite these high-frequency modes with a significant probability. Moreover, since these modes are polarized parallel to the surface, their coupling to the helium atoms is much weaker than for the sagittal plane modes. The quasi-acoustic mode  $A_1$  in the calculated curves is assigned to the  $E_1$  branch. It corresponds mainly to parallel  $x$  and  $y$  translations, with, however, a significant hybridization with the perpendicular  $z$  vibration near the  $\bar{\Gamma}$  point, while it becomes fully perpendicularly polarized at the end of the first Brillouin zone. In the same way, it might be obvious to assign the phonon dispersion curve  $A_2$  calculated around 6.5 meV to the observed  $E_2$  mode.  $A_2$  is polarized mostly perpendicular to the surface and corresponds to the vibration in the  $z$  direction. However, as shown in Sec. III, from the intensity analysis there is strong evidence that mode  $E_2$  has significant contributions from motions in the  $x$  and  $y$  direction, corresponding to parallel vibrations. Since the modes  $A_3$ - $A_6$  show very significant polarization parallel to the surface, this result may indicate that the experimentally observed  $E_2$  mode is actually a mixture of the  $A_2$  with other phonons.

Based on the calculations, the observation of the  $E_3$  mode in the range 8–10 meV is somewhat surprising since it is assigned to the  $x$  and  $y$  vibrations of the admolecule centers of mass parallel to the surface (mode  $A_4$  in the calculations). However, the dynamical coupling with the substrate, which leads to avoided crossings between the adlayer and substrate curves could change the polarization of the modes through hybridizations with the perpendicularly polarized folded branch of the Rayleigh surface mode. This may explain why this mode, which is a purely parallel mode when no coupling with the substrate dynamics is considered, becomes visible after hybridization with the substrate modes.

The modes  $A_7$  and  $A_8$  around 13 meV, which are assigned to  $\theta$  motions perpendicular to the surface, can be connected to the  $E_4$  branch. Finally, part of the experimental points nicely coincides with the substrate Rayleigh mode (lowest of the dashed lines in Fig. 7).

These phonon-libron dispersion curves for the  $C_2H_2/KCl$  system can be compared with previous results obtained for the same adsorptive on NaCl. In this latter case, the phonon modes have been studied only for the low-density ( $3\sqrt{2} \times \sqrt{2}$ ) $R45^\circ$  phase containing four molecules per unit cell.<sup>21</sup> The layer dynamics of  $C_2H_2$  on the two substrates present some similarities. However, on NaCl(001) only two

modes were observed the first one between 7 and 9 meV ( $E'_1$ ) and the second one around 14 meV ( $E'_2$ ). They were assigned to perpendicular  $z$  vibrations and  $\theta$  librations, respectively. These dispersionless modes, which are mainly sensitive to the interaction with the surface, are also observed and assigned in the present study with yet slightly lower frequencies, due to the greater softness of the molecule-KCl force constants. The main difference between the two substrates comes from the modes assigned to the  $x$  and  $y$  parallel translations. Indeed, on NaCl, these modes are nearly dispersionless and, due to their parallel polarization, are not visible in HAS experiments. On the contrary, a strongly dispersive branch  $E_1$  is observed on KCl at low frequency and assigned to parallel translations (mode  $A_1$ ), as the result of a much higher  $C_2H_2$  density in the monolayer on KCl. Since the parallel translations are very sensitive to the strength of the lateral force constants, it is not surprising to have a stronger dispersion and a larger energy for this mode when the density is higher. Due to this larger energy and dispersion on KCl, the  $A_1$  mode is thus cut by the folded part of the Rayleigh substrate mode, which changes its polarization and makes it better visible in HAS experiments ( $E_1$  branch). Since the polarization of the  $A_1$  mode changes and its energetic position is close to the  $A_2$  mode in the second half of the Brillouin zone, it is not obvious to give an interpretation of the experimentally observed intensities. Nevertheless, the observed decrease in intensity out to the zone boundary agrees with the polarization character found theoretically. However, this assignment cannot alone explain the strong dispersion of the mode.

The ordering of  $C_2H_2$  molecules on KCl, which leads to the formation of a complete monolayer with low order commensurability, is consistent with the better registry of the adsorbate/substrate lattice parameters for the system  $C_2H_2/KCl$  (2%) than for  $C_2H_2/NaCl$  (8%). The corresponding larger coverage in adsorbate molecules for KCl is consistent with the  $\omega_\lambda(\mathbf{q})$  curves of the  $C_2H_2$  monolayer, which are clearly more dispersive for the KCl substrate, indicating a larger influence of the attractive lateral force constants between admolecules.

## VII. CONCLUSIONS AND OUTLOOK

Following up on a recent study of the monolayer phases of acetylene on NaCl(001) the monolayer acetylene on KCl(001) has been investigated experimentally by helium atom scattering and theoretically by potential energy calculations. A complete monolayer has been found with  $(\sqrt{2} \times \sqrt{2})R45^\circ$  geometry and glide planes along the [100] and [010] directions, with a unit cell of two translationally inequivalent molecules, which lie flat on the surface. The experimental phonon dispersion curves of the monolayer are in good agreement with the calculated spectra, which allow an assignment of all measured modes. Compared to the adsorbate acetylene on NaCl stronger dispersion is observed, which is supposed to be due to the higher molecular density of  $C_2H_2/KCl$ , where lateral interactions become more important. Another consequence of this fact is, that, in contrast to  $C_2H_2/NaCl$  the initially parallel  $A_1$  mode undergoes a change in polarization and becomes easily visible for HAS.

The small mismatch in lattice parameters between  $C_2H_2$

and KCl opens up the possibility of the adsorption of ordered multilayers, which might have very similar properties to a pure acetylene crystal. Indeed, by isothermal adsorption at a surface temperature of  $T_s=40$  K, layer-by-layer growth could be observed for at least 15 layers, which occurs rarely for physisorbates on ionic crystals, the only other system that

has been reported being  $\text{CH}_4$  on  $\text{MgO}$ .<sup>39,40</sup> Elastic and inelastic He-scattering measurements have been performed on these crystalline films as well as molecular dynamics simulations of the first five layers of such multilayer adsorbates. The analysis is still in progress and will be presented in a forthcoming paper.<sup>41</sup>

- <sup>1</sup>H. C. Chang, H. H. Richardson, and G. E. Ewing, *J. Chem. Phys.* **89**, 7561 (1988).
- <sup>2</sup>D. Schmicker, J. P. Toennies, R. Vollmer, and H. Weiss, *J. Chem. Phys.* **95**, 9412 (1991).
- <sup>3</sup>J. Heidberg, E. Kampshoff, and M. Suhren, *J. Chem. Phys.* **95**, 9408 (1991).
- <sup>4</sup>S. K. Dunn and G. E. Ewing, *J. Phys. Chem.* **96**, 5284 (1992).
- <sup>5</sup>P. Audibert, M. Sidoumou, and J. Suzanne, *Surf. Sci. Lett.* **273**, L467 (1992).
- <sup>6</sup>J. Heidberg, B. Redlich, and D. Wetter, *Ber. Bunsenges. Phys. Chem.* **99**, 1333 (1995).
- <sup>7</sup>A. Glebov, R. E. Miller, and J. P. Toennies, *J. Chem. Phys.* **106**, 6499 (1997).
- <sup>8</sup>D. Ferry, S. Picaud, P. N. M. Hoang, C. Girardet, L. Giordano, B. Demirdjian, and J. Suzanne, *Surf. Sci.* **409**, 101 (1998).
- <sup>9</sup>B. Wassermann, S. Mirbt, J. Reif, J.C. Zink, and E. Matthias, *J. Chem. Phys.* **98**, 10 049 (1993).
- <sup>10</sup>C. Girardet, S. Picaud, and P. N. M. Hoang, *Europhys. Lett.* **25**, 131 (1994).
- <sup>11</sup>W. Langel and M. Parrinello, *Phys. Rev. Lett.* **73**, 504 (1994).
- <sup>12</sup>L. W. Bruch, A. Glebov, J. P. Toennies, and H. Weiss, *J. Chem. Phys.* **103**, 5109 (1995).
- <sup>13</sup>A. W. Meredith and A. J. Stone, *J. Chem. Phys.* **104**, 3058 (1996).
- <sup>14</sup>K. Jug and G. Geudtner, *Surf. Sci.* **371**, 95 (1997).
- <sup>15</sup>A. Allouche, *Surf. Sci.* **374**, 117 (1997); **406**, 279 (1998).
- <sup>16</sup>J. Ahdjoudj and C. Minot, *Surf. Sci.* **402-404**, 104 (1998).
- <sup>17</sup>P. N. M. Hoang, S. Picaud, C. Girardet, and A. W. Meredith, *J. Chem. Phys.* **105**, 8453 (1996).
- <sup>18</sup>P. N. M. Hoang, S. Picaud, and C. Girardet, *Surf. Sci.* **360**, 261 (1996).
- <sup>19</sup>C. Girardet, P. N. M. Hoang, and S. Picaud, *Phys. Rev. B* **53**, 16 615 (1996).
- <sup>20</sup>S. Picaud, C. Girardet, A. Glebov, J. P. Toennies, J. Dohrmann, and H. Weiss, *J. Chem. Phys.* **106**, 5271 (1997).
- <sup>21</sup>S. Picaud, P. N. M. Hoang, C. Girardet, A. Glebov, R. E. Miller, and J. P. Toennies, *Phys. Rev. B* **57**, 10 090 (1998).
- <sup>22</sup>W. G. Wyckoff, *Crystal Structures* (Wiley, New York, 1968), Vol. 1.
- <sup>23</sup>R. K. McMullan, Å. Kvik, and P. Popelier, *Acta Crystallogr., Sect. B: Struct. Sci.* **48**, 726 (1992).
- <sup>24</sup>J. P. Toennies and R. Vollmer, *Phys. Rev. B* **44**, 9833 (1991); R. Vollmer, Ph.D. thesis, MPI für Strömungsforschung, 1992.
- <sup>25</sup>G. Lange, D. Schmicker, J. P. Toennies, R. Vollmer, and H. Weiss, *J. Chem. Phys.* **103**, 2308 (1995).
- <sup>26</sup>J. Heidberg, G. Lange, O. Schönekas, J. P. Toennies, and H. Weiss, *Ber. Bunsenges. Phys. Chem.* **99**, 1370 (1995).
- <sup>27</sup>D. Ferry, A. Glebov, V. Senz, J. Suzanne, J. P. Toennies, and H. Weiss, *Surf. Sci.* **377-379**, 634 (1997).
- <sup>28</sup>G. Brusdeylins, R. B. Doak, and J. P. Toennies, *Phys. Rev. B* **27**, 3662 (1983).
- <sup>29</sup>D. Ferry and J. Suzanne, *Surf. Sci.* **345**, L19 (1996).
- <sup>30</sup>A. J. Stone, *Chem. Phys. Lett.* **83**, 233 (1981).
- <sup>31</sup>A. J. Stone and M. Alderton, *Mol. Phys.* **56**, 1047 (1985).
- <sup>32</sup>A. J. Stone, *The Theory of Intermolecular Forces* (Clarendon, Oxford, 1996).
- <sup>33</sup>S. S. Sung and P. C. Jordan, *J. Chem. Phys.* **85**, 4045 (1986).
- <sup>34</sup>P. N. M. Hoang, C. Girardet, M. Sidoumou, and J. Suzanne, *Phys. Rev. B* **48**, 12 183 (1993).
- <sup>35</sup>V. Pouthier, C. Ramseyer, and C. Girardet, *Surf. Sci.* **382**, 349 (1997).
- <sup>36</sup>M. P. Allen and D. J. Tildesley, *Computer Simulations of Liquids* (Clarendon, Oxford, 1987).
- <sup>37</sup>A. Marmier, P. N. M. Hoang, S. Picaud, C. Girardet, and R. M. Lynden-Bell, *J. Chem. Phys.* **109**, 3245 (1998).
- <sup>38</sup>Z. Gamba and H. Bonadeo, *J. Chem. Phys.* **76**, 6215 (1982).
- <sup>39</sup>M. Bienfait, *Europhys. Lett.* **4**, 79 (1987).
- <sup>40</sup>J. P. Coulomb, M. Maclih, B. Croset, and H. J. Lauter, *Phys. Rev. Lett.* **54**, 1536 (1985).
- <sup>41</sup>L. W. Bruch, C. Girardet, A. L. Glebov, P. N. M. Hoang, S. Picaud, J. P. Toennies, F. Traeger, and H. Weiss (unpublished).